ARTICLE

BIOTECHNOLOGY and BIOENGINEERING

Kinetic Model of a Granular Sludge SBR: Influences on Nutrient Removal

M.K. de Kreuk,[1] C. Picioreanu,[1] M. Hosseini,[1] J.B. Xavier,[2] M.C.M. van Loosdrecht[1]

[1]Department of Biotechnology, Delft University of Technology, Julianalaan 67, 2628BC Delft, The Netherlands; telephone: 0031-15-2781551; fax: 0031-15-2782355; e-mail: m.k.dekreuk@tudelft.nl

[2]Biomathematics group, Instituto de Technologia Química e Biológica, Universidade Nova Lisboa, R. Qta Grande 6, 2780 Oeiras, Portugal

Received 23 May 2006; accepted 25 August 2006

Published online 18 December 2006 in Wiley InterScience (www.interscience.wiley.com). DOI 10.1002/bit.21196

ABSTRACT: A mathematical model was developed that can be used to describe an aerobic granular sludge reactor, fed with a defined influent, capable of simultaneously removing COD, nitrogen and phosphate in one sequencing batch reactor (SBR). The model described the experimental data from this complex system sufficiently. The effect of process parameters on the nutrient removal rates could therefore be reliably evaluated. The influence of oxygen concentration, temperature, granule diameter, sludge loading rate, and cycle configuration were analyzed. Oxygen penetration depth in combination with the position of the autotrophic biomass played a crucial role in the conversion rates of the different components and thus on overall nutrient removal efficiencies. The ratio between aerobic and anoxic volume in the granule strongly determines the N-removal efficiency as it was shown by model simulations with varying oxygen concentration, temperature, and granule size. The optimum granule diameter for maximum N- and P-removal in the standard case operating conditions (DO 2 mg L^{-1}, 20°C) was found between 1.2 and 1.4 mm and the optimum COD loading rate was 1.9 kg COD m^{-3} day^{-1}. When all ammonia is oxidized, oxygen diffuses to the core of the granule inhibiting the denitrification process. In order to optimize the process, anoxic phases can be implemented in the SBR-cycle configuration, leading to a more efficient overall N-removal. Phosphate removal efficiency mainly depends on the sludge age; if the SRT exceeds 30 days not enough biomass is removed from the system to keep effluent phosphate concentrations low.

Biotechnol. Bioeng. 2007;97: 801–815.

KEYWORDS: aerobic granular sludge; modeling; nutrient removal; SBR; simultaneous nitrification/denitrification (SND); P-removal

Introduction

Aerobic granular sludge technology is a new and promising development in the field of aerobic wastewater treatment. This technology is based on sequencing batch reactors (SBRs), with a cycle configuration chosen such that a strict selection occurs for fast settling aerobic granules and that these granules are oxygen limited instead of substrate limited. This leads to the growth of stable and dense granules under anaerobic/aerobic conditions (De Kreuk et al., 2005a; Dulekgurgen et al., 2003; Li et al., 2005). Compared to conventional activated sludge systems, a system based on aerobic granular sludge has several advantages, namely compactness, lower operational and construction costs and lower energy requirement. Many laboratory studies (among others Beun et al., 1999; Liu and Tay, 2004; Morgenroth et al., 1997; Tay et al., 2002), a feasibility study (De Bruin et al., 2004) and a pilot study (De Bruin et al., 2005) showed the potential of aerobic granular sludge SBRs, and the next step is to apply this technology in practice.

Mathematical modeling has proven very useful to study complex processes, such as the aerobic granular sludge systems (Beun et al., 2001; Lübken et al., 2005). Biological processes in the granules are determined by concentration gradients of oxygen and diverse substrates. The concentration profiles are the result of many factors, for example, diffusion coefficients, conversions rates, granule size, biomass spatial distribution, and density. All of these factors tightly influence each other, thus the effect of separate factors cannot be studied experimentally. Moreover, due to the long sludge age in granule systems (usually up to 70 days, De Kreuk and Van Loosdrecht, 2004), lengthy experiments should be carried out before we can speak of a steady state approaching system. Therefore, a good

Correspondence to: M.K. de Kreuk

Contract grant sponsors: STOW; STWA; FCT/MCTES, Portugal
Contract grant numbers: TNW99.262; DPC5577; SFRH/BPD/11485/2002

computational model for the granular sludge process provides significant insight in the most important factors that affect the nutrient removal rates and in the distribution of different microbial populations in the granules. Further, the model could also be used for process optimization and for the scale-up and design of a full-scale reactor for the new aerobic granular sludge technology (or *Nereda*^{TM}).

The computational model used in this study is based on previously developed models. The SBR and granular sludge descriptions are principally as in the model of Beun et al. (2001), which described heterotrophic organisms storing acetate (without phosphate accumulation) in a feast-famine regime in combination with autotrophic organisms for nitrogen removal. Because the design of Nereda^{TM} aims at phosphate removal via the selection of slow growing phosphate accumulating organisms (PAO), the existing aerobic granular sludge model was extended with conversion processes involving PAO as described in the models of continuous activated sludge systems by Hao et al. (2001) and Meijer (2004). The results from the present model simulations are compared here to different laboratory scale experiments. This model will be used here for evaluation of the overall reactor performance only. A detailed modeling study of the population dynamics within aerobic granular sludge is described in Xavier et al. (Submitted).

Materials and Methods

Laboratory Scale Set-Up

Experiments were performed in 3 L SBRs (internal diameter 6.25 cm) operated as bubble column (SBBC) or airlift reactor (SBAR). Air was introduced via a fine bubble aerator at the bottom of the reactors (4 L/min). Dissolved oxygen (DO) was measured as percentage of oxygen saturation and could be controlled via adding N_2 or air to the recirculation flow of the off gas through the reactor. pH was maintained at 7.0 ± 0.2 by dosing 1 M NaOH or 1 M HCl. Hydraulic retention time was 5.6 h and the substrate load, measured in chemical oxygen demand (COD), was 1.6 kgCOD $m^{-3}day^{-1}$.

The reactors were operated in successive cycles of 3 h: 60 min of anaerobic feeding from the bottom of the reactor; 112 min aeration; 3 min settling; 5 min effluent discharge.

The composition of the influent media were (A) Na acetate 63 mM, $MgSO_4{\cdot}7H_2O$ 3.6 mM, KCl 4.7 mM and (B) NH_4Cl 35.4 mM, K_2HPO_4 4.2 mM, KH_2PO_4 2.1 mM, and 10 ml/L trace element solution. From each medium (A and B) 0.15 L per cycle were dosed together with 1.3 L tap water.

Exact methods for reactor operation, trace element solution, and measurement of the experimental data used for model calibration and comparison are described in De Kreuk et al. (2005a,b).

Model Description

The mathematical model describing the performance of the laboratory-scale granular sludge SBR was implemented in the well-established AQUASIM simulation software for environmental applications (Reichert, 1998). A combination of completely mixed reactor and biofilm reactor compartments (based on Wanner and Gujer, 1986, provided by AQUASIM, was used to simulate the mass transport and conversion processes occurring in the bulk liquid and in the granules of the SBR system. The biological conversion processes are described using stoichiometric and kinetic parameters from the models published by Hao et al. (2001, 2002b)) and Meijer (2004).

The model was used to simulate the conversion processes that occur in a laboratory scale reactor and compare them with those obtained experimentally under the same conditions. Furthermore, it was used to predict the nutrient removal efficiencies under different circumstances. Special attention has been paid to the distribution of the different microbial species in the granules, as resulting from the model simulations. This distribution, in combination with the oxygen penetration depth, gives insight in the overall reactor performance and its sensitivities.

Conversion Processes

The model accounts for biomass distribution among seven particulate components (Fig. 1). Three active biomass types include the phosphate-accumulating organisms (X_{PAO}) and the nitrifiers (ammonia-oxidizers, X_{NH} and nitrite-oxidizers, X_{NO}). One inactive biomass component (X_I) was defined. Special pools are defined for internally stored biomass: polyphosphate (X_{PP}), poly-hydroxybutyrate (X_{PHB}), and glycogen (X_{GLY}). Seven dissolved components are considered relevant for the biological conversions and process stoichiometry: oxygen (S_{O_2}), acetate (S_{Ac}), ammonium (S_{NH_4}), nitrite (S_{NO_2}), nitrate (S_{NO_3}), nitrogen (S_{N_2}), and phosphate (S_{PO_4}).

It was assumed that acetate would be consumed by PAO and converted to a storage polymer (polyhydroxybutyrate,

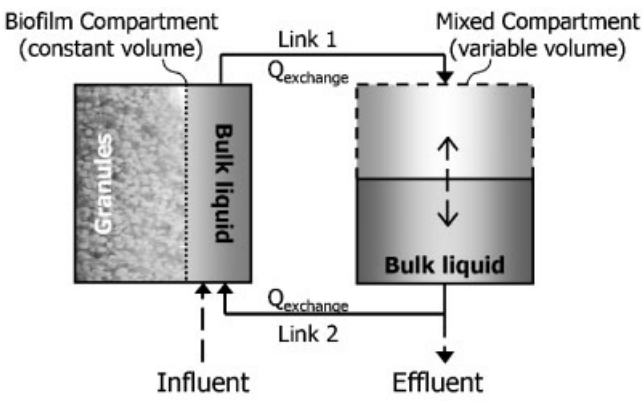

Figure 1. Schematic representation of the model set-up in AQUASIM. Each compartment contains 7 soluble components (S_{O_2}, S_{Ac}, S_{NH_4}, S_{NO_2}, S_{NO_3}, S_{PO_4}, S_{N_2}) and 7 particulate components (X_{PAO}, X_{NH}, X_{NO}, X_I, X_{PP}, X_{PHB}, X_{GLY}) involved in 21 metabolic processes. All soluble and particle components are found in effluent and recirculation links.

DOI 10.1002/bit

PHB) during the anaerobic period. Converting glycogen and degrading poly-P generate energy needed for the active uptake of acetate. During the aerobic period, the stored PHB is used for growth, maintenance and restoring the glycogen and poly-P pools. The formation of glycogen and the formation of poly-P are always coupled to the consumption of PHB and therefore, these aerobic or anoxic processes cannot be read separately. In the aerobic period, also nitrification takes place, with ammonia converted via nitrite into nitrate. All anoxic processes can take place on nitrite and nitrate as electron acceptors, depending on their availability. Also endogenous respiration for autotrophic organisms is included. When no PHB, glycogen nor acetate is available, PAO will decay. For simplicity and to maintain the granule structure, the decayed biomass was considered to be turned into inert material (Beun et al., 2001). To limit the calculation time for the simulation, no other heterotrophic organisms (X_H) were included in the model. This is justified by the fact that a very small amount of the incoming acetate is left at the start of the aerobic period, which could be consumed by aerobic heterotrophs and by PAO (Fig. 2). The lack of acetate during the aerobic period will limit the growth and will result in the total disappearance of heterotrophic organisms other than the ones capable of anaerobically storing substrate (as shown by Xavier et al., Submitted). Therefore, omitting the heterotrophs that do not store substrate is not expected to greatly influence the long-term (''steady-state'') simulation results.

The stoichiometry and kinetics of biological conversions are derived from the Delft bio-P model for activated sludge (Meijer, 2004; Murnleitner et al., 1997; van Veldhuizen et al., 1999) and presented with the Activated Sludge Model (ASM) notation (Henze et al., 1999) in Appendix 1.

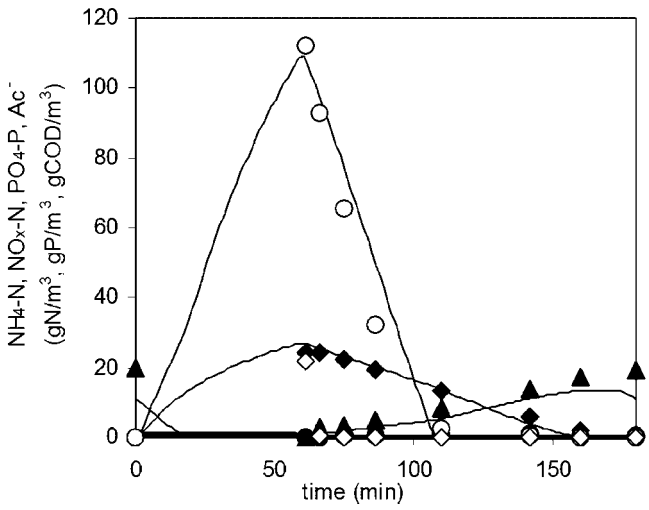

Figure 2. Measured concentrations during a cycle measurement (points; PO_4-P (○), Acetate (◇), NH_4-N (◆), NO_3-N (▲), NO_2-N (●)) and simulated results with the present model (lines), in the standard case (DO 2 mg·L^{-1}, 20°C, granule diameter 1.1 mm).

Stoichiometric and kinetic parameter values are given in Appendix 2 and Appendix 3, respectively. A few model parameters were altered with respect to the original models, as can be read from the reference column of these Appendices.

Since only one kinetic model describes all the different processes and the experimental results in both the aerobic granules and in the reactor, the following parameters needed to be adjusted. The reduction factor for process rates under anoxic conditions (η) was chosen 0.3, since this described best the experimentally measured values for nitrate production. This low reduction value is needed, because in this model denitrification can occur on both nitrite and nitrate. In other models, denitrification often only takes place on nitrate. Allowing denitrification with nitrate and nitrite simultaneously and not adding an inhibition factor for the preference of one of the two electron acceptors would double the denitrification rates, producing unrealistic results if no reduction factor (η) was used.

Part of the phosphate removal in aerobic granular sludge is removed by (biologically induced) precipitation (De Kreuk et al., 2005a). For simplicity, precipitation was not included in the model. As an alternative, the maximum fraction of poly-phosphate (f_{PP}^{max}) was increased from 0.35 (Wentzel et al., 1989) to 0.65. Consequently, the maximum fraction of stored PHB had to be adjusted in order to generate enough PHB for the increased poly-P uptake.

Another model adjustment concerns the expressions for the reaction rates. In order to prevent the occurrence of negative values for solute concentrations, switch functions were used (Appendices 1 and 3). These continuous S-shaped functions shut down a process consuming a reactant whose concentration is nearly zero and, in this way, make the simulations numerically more stable.

Reactor Description

Liquid circulation pattern. In the laboratory scale SBR, influent is fed from the bottom of the reactor with a flow pattern close to plug flow through the settled bed of granules (De Kreuk and Van Loosdrecht, 2004). At the end of each cycle, the effluent is discharged from a port at half of the reactor height. The AQUASIM software does not allow the volume of the bulk liquid in the biofilm compartment to vary in time. In order to circumvent this and simulate the fill and discharge process, two linked compartments have to be defined. A completely mixed liquid compartment with variable volume is connected to the biofilm compartment. A high fluid circulation rate ($Q_{exchange}$) between the two compartments ensures the same bulk liquid concentrations in both compartments (Fig. 1).

We chose to represent the flow pattern in the reactor as completely mixed because the simulation in AQUASIM of different liquid circulation regimes in different phases of the SBR cycle would imply enormous difficulties. It is expected that the liquid circulation in the feeding phase affects the

diffusion rate of acetate into the granule. Consequently, it also determines the stored substrate in the anoxic interior of the granules available for denitrification during the aerobic period (simultaneous nitrification/denitrification, SND). With a plug-flow feeding pattern, the substrate concentration in the lowest part of the settled granule bed is equal to the influent substrate concentration. In the model, however, the influent is directly mixed with the remaining bulk liquid in the reactor, leading to a decreased concentration in the bulk liquid surrounding the granules. To compensate for this lower substrate concentration, the diffusion coefficient of acetate in the AQUASIM model during feeding was increased arbitrarily.

Cyclic SBR operation. The model biofilm compartment contains a biofilm volume, which accounts for all the granules and bulk liquid volume (Fig. 1). The volume of this compartment was fixed at 1.5 L. The completely mixed compartment contained the remainder of the liquid volume in the system, with a maximum volume of 1.6 L. The influent (1.5 L) entered the reactor in the biofilm compartment during the first 60 min of the cycle. In the model, aeration of the bulk liquid was switched on during the next 112 min (3 h cycle) or 232 min (4 h cycle). The last 8 min of the cycle effluent is discharged from the mixed compartment. Other parameters needed for the AQUASIM model are given in Appendix 4.

Number and size of granules. The number of granules, in combination with the granule diameter, can affect the outcome of the simulation, because this influences the overall liquid/granule interfacial area. The granules grown in the laboratory had the following characteristics: granule size distribution between 0.36 and 3.7 mm (average diameter 1.1 mm, standard deviation 0.45); aspect ratio 0.72; shape factor 0.74; dry weight in reactor 18 $gVSS \cdot L^{-1}$; ash content 37%; SVI_8 15 $mL \cdot g^{-1}$ (De Kreuk et al., 2005b). The laboratory reactor contains thus a wide variation in granule sizes, which also change in time. However, the use of a system with a granule size distribution was avoided in this model, since it would significantly increase the complexity of the numerical computations and it is not expected to contribute to a better understanding of the system. Therefore, in the simulations the diameter chosen was 1.1 mm, which is the most representative for aerobic granules in our reactor. The number of granules was set to 600,000, resulting in a comparable amount of biomass as present in the laboratory scale reactor. The sensitivity of the size and the number of granules was evaluated in several simulations. A radius-dependent biofilm area was set in AQUASIM to correctly represent the spherical symmetry of the granules.

Simulation Strategy

Since experimental data measured during one cycle are different in time, depending on granule size, morphology and reactor operation, a representative cycle measurement was chosen to compare to a standard simulation case (Fig. 2). This simulation case was performed under the same operational conditions as applied during this standard operation of the SBR. The DO was controlled at 2 $mg \cdot L^{-1}$ during the aerobic phase, the temperature was 20°C and influent concentrations were as given in Table 4. The initial concentrations of the biomass in the granule were: PAO (X_{PAO}) 50,000 $gCOD \cdot m^{-3}$; ammonia oxidizers (X_{NH}) and nitrite oxidizers (X_{NO}) 5,000 $gCOD \cdot m^{-3}$ each; inerts (X_I) 1 $gCOD \cdot m^{-3}$; glycogen concentration (X_{GLY}) 22,500 $gCOD \cdot m^{-3}$; PHB concentration (X_{PHB}) 36,000 $gCOD \cdot m^{-3}$; poly-P concentration (X_{PP}) 29,250 $gP \cdot m^{-3}$ (initial concentration of the storage polymers was set to 90% of the maximum fraction). These initial values were based on the overall density of aerobic granular sludge (80 $gTSS \cdot L^{-1}$) and a sufficient amount of storage polymers for the conversions.

The operation of the SBR under different conditions (such as changed DO concentrations, the influence of granule diameter and of sludge load) was simulated for 365 days, which corresponds to about 8 h of computing time on a Pentium 4, 2.4 GHz processor. After 200 days of simulation, the effluent concentrations were compared at a 5 days interval. The fluctuations of effluent concentrations over these intervals were less than 1%. Inside the simulated granule, in the outer layer from radius 0.22 to 0.55 mm (87.5% of the volume of the granule), the biomass concentration did not change more than 1% per 5 days after 350 days of simulation. In the inner zone of the granule (radius 0–0.22 mm) the biomass concentrations of the autotrophic organisms changed with less than 4% per 5 days. These results showed that, in the simulations, after 365 days the reactor effluent and the granule composition could be considered sufficiently close to a steady state. In the experiments at laboratory scale, measurements are mostly performed between 4 months and 1.5 years after an operation change, which is in agreement with the simulated 365 days of operation.

Results

Standard Case: Evaluation of the Model With Experimental Data

The standard operation of the granule reactor was simulated first. The results of this simulation, in steady state reached after 365 days, are shown in Figure 2, together with the concentrations measured in the laboratory scale reactor during a cycle with the same operational conditions. Conversion rates measured in the experiments were compared to the ammonium and phosphate consumption and to the net nitrite and nitrate production rates obtained from the model. Maximum conversion rates observed in the experiments were determined by taking the largest slope of at least three data points in the cycle. This was compared to the average conversion rate over the same time interval in the simulation. The conversion rates resulting from the model in this standard case did not differ with more than

DOI 10.1002/bit

Table I. Effect of dissolved oxygen concentration on the overall N- and P-removal rates in the SBR during short- and long-term changes (standard case in italic).

	Overall net conversion rates ($mg\text{-}N \cdot L^{-1} \cdot h^{-1}$, $mg\text{-}P \cdot L^{-1} \cdot h^{-1}$)			
	NH_4^+ consumption	NO_2^- production	NO_3^- production	PO_4^{3-} consumption
DO concentration 1 mg/L (one cycle change)	7.2 (8.5)	0 (0)	1.5 (0)	98 (144)
DO concentration 2 mg/L (long-term operation)	15.9 (18.0)	1.1 (1.1)	10.0 (14.4)	142 (156)
DO concentration 4 mg/L (long-term operation and start for the one-cycle changes)	*23.1 (15.1)*	*0 (0.2)*	*16.4 (2.4)*	*173 (199)*
DO concentration 10 mg/L (one cycle change)	28.8 (19.4)	1.0 (n.a.)	26.0 (20.2)	197 (267)
DO concentration 10 mg/L (long-term operation)	31.9 (15.4)	1.2 (1.7)	26.1 (22.5)	193 (202)

The short-term changes are simulated with the biomass distribution as developed after 365 days at DO 4 mg/L. Rates are calculated from the slopes of the simulated and experimentally determined concentration profiles in the reactor during a cycle. Experimental data are shown between parentheses (De Kreuk et al., 2005a).

30% from the values found in the experiments (Table I, first row). Given all the uncertain parameters (e.g., exact granule size distribution and granule surface area), it was concluded that the model described the experimental data satisfactorily. Default parameters were thereby considered to be good enough not to calibrate the model any further and to start performing other simulations in different operational conditions. For this reason, the parameter values for this standard case are used to obtain all other results, unless mentioned otherwise.

Short- and Long-Term DO Changes

To study the effects of short- and long-term DO changes, the DO was varied for different series of model simulations and the results were compared with data from laboratory experiments (De Kreuk et al., 2005a). For long-term effects, the development of granular sludge was simulated during 365 days of reactor operation at DO concentrations of 2, 4, and 10 $mg \cdot L^{-1}$. The results of the 4 $mg \cdot L^{-1}$ simulation were then used to simulate short-term effects of a DO shift during one cycle to 1 $mgO_2 \cdot L^{-1}$ and to 10 $mgO_2 \cdot L^{-1}$, respectively. Due to the relatively short-time interval during these DO shifts, the biomass distribution within the granule did not significantly change.

Conversion rates obtained experimentally and by simulation, are given in Table I. The conversion rates for the short-term experiments show the same trend. At an increased DO most rates are enhanced. Ammonium is consumed faster, while the net nitrate production rate increased even more, due to lower denitrification rates in the presence of high oxygen concentration.

The simulated biomass distribution in a granule grown at 2 and 10 mg $O_2 \cdot L^{-1}$ and the oxygen penetration depths during the cycle are compared in Figure 3a–f. The increased oxygen penetration depth during the total aeration period (DO 10 mg/L) reduced the competition for oxygen between autotrophs and PAO in the outer layer and created the possibility for autotrophic organisms to accumulate in the inner zones of the granule. This increased concentration of autotrophs enhanced the nitrification rates at higher oxygen concentrations (Table I), however, because an anoxic zone was lacking the total N-removal efficiency decreased. At 2 $mgO_2 \cdot L^{-1}$ the simulated total N-removal efficiency was 60% (61% in the experimental data-set), while at 10 $mgO_2 \cdot L^{-1}$ it was only 33% (10% in the experimental data-set). The ammonia consumption rate at higher oxygen concentrations is particularly overestimated in the model simulations, especially for the long-term oxygen change. These higher N-removal rates and efficiencies obtained from the model simulations compared to the experiments can be explained by the lower biomass concentration present in the reactor during the experiments at 10 mg $O_2 \cdot L^{-1}$ (16 $gTSS \cdot L^{-1}$ vs. 28 $gTSS \cdot L^{-1}$ during the experiment at 2 $mgO_2 \cdot L^{-1}$, later TSS value was used for model calibration).

The phosphate removal at higher oxygen concentrations is faster than at low oxygen concentrations. This is due to the significantly faster storage of Poly-P in aerobic conditions than in anoxic conditions. At higher oxygen concentrations and thus at an increased oxygen penetration depth in the granules, more PAO will be able to store their phosphate aerobically, resulting in an increased P-removal rate. At all simulated oxygen concentrations here, the storage was high enough to have complete phosphate removal.

The Influence of Temperature

Variations in process temperature (20, 15, and 8°C) were simulated according to experiments performed in a laboratory scale reactor. Starting with the steady state data of the standard case simulation at 20°C (2 mg $O_2 \cdot L^{-1}$), temperature was lowered to 15°C and the process was simulated for 50 more days. Subsequently, the temperature was lowered again to 8°C followed by an additional simulation of 65 days. Both simulated periods were equal to the duration of the long-term temperature change experiments (De Kreuk et al., 2005b). Short-term temperature shift experiments were also simulated by changing the temperature to 15 and 8°C during two cycles each. Especially the simulated biomass distribution in the long-term low temperature experiments was of interest, since experiments suggested an enrichment of autotrophic organisms in deeper layers of the granules at low temperatures. Simulations

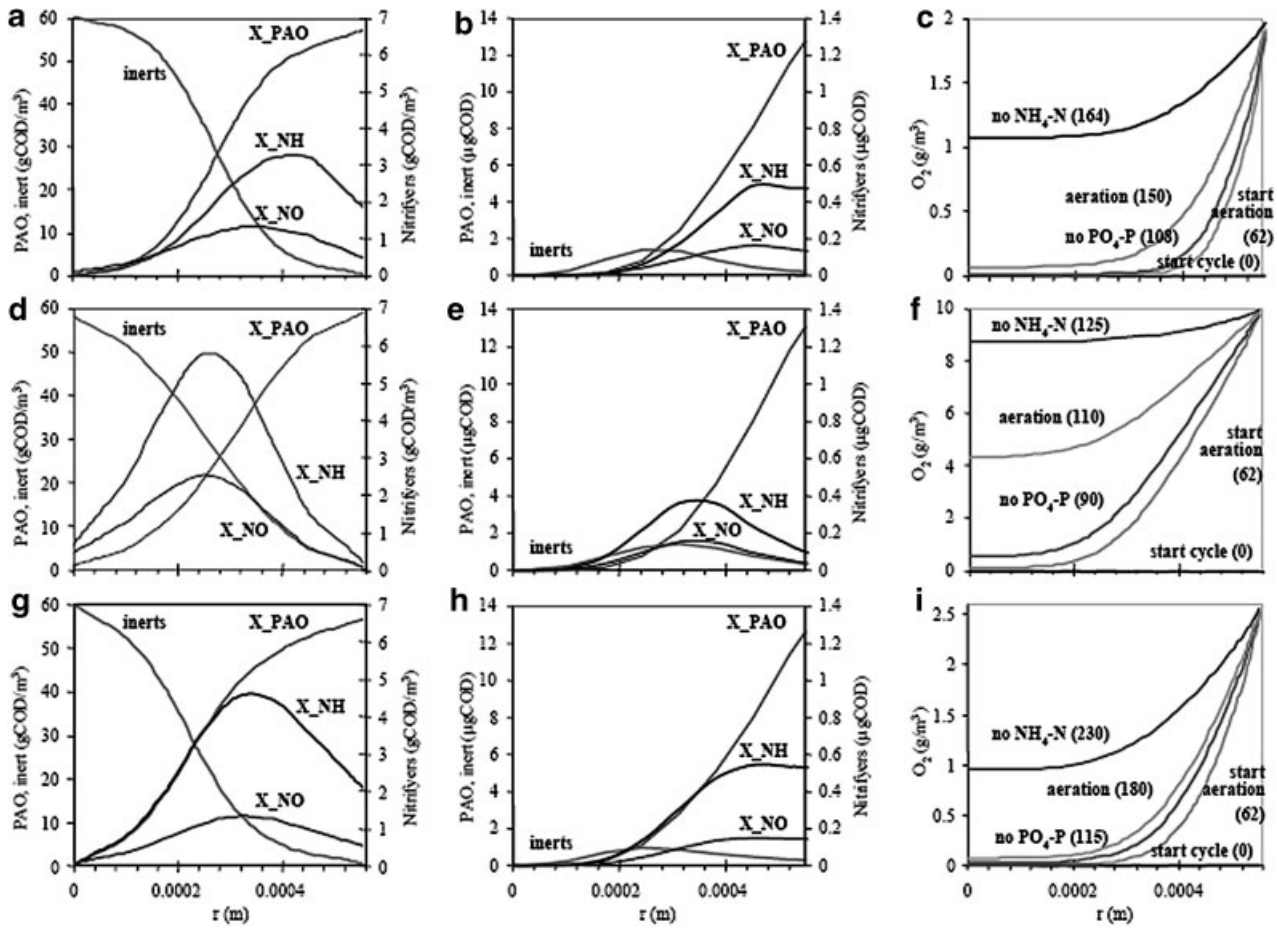

Figure 3. Distribution of biomass concentration in the granules (**a**, **d**, **g**), the absolute quantity of biomass at different positions inside the granules (**b**, **e**, **h**) and the oxygen profile inside the granules at different moments in a cycle, cycle times (minutes) between brackets (**c**, **f**, **i**). Oxygen concentration in the bulk liquid was set at 2 mg·L^{-1} (a, b, c) and10 mg·L^{-1} (d, e, f) with a temperature of 20°C during 365 days simulation. The temperature set to 8°C with an oxygen concentration maintained at 2.6 mg·L^{-1} (DO 20% saturation) during 80 days of simulation (g, h, i).

indicated that this accumulation of autotrophs was mainly due to a higher oxygen penetration depth, caused by decreased activity in the outer layers of the granules.

The results of the simulations were largely according to those expected from the experiments (Table II). Figure 3g–h shows an increased amount of ammonia oxidizing bacteria in the granules simulated at 8°C. This results in a higher ammonia consumption rate in the long-term simulation at 8°C compared to the short-term simulated shift. These rates are similar to the ones found in the experiments (Table II). Consistently, the N- and P-removal rates are significantly lower after short temperature shifts compared to the long-term shifts, both in experiments and in simulations. However, it can be seen that the rates of 20 and 15°C

Table II. Effect of temperature on the overall N- and P-removal rates in the SBR, during short- and long-term changes (standard case in italic).

	Overall net conversion rates (mg-N · L^{-1} · h^{-1}, mg-P · L^{-1} · h^{-1})			
	NH_4^+ consumption	NO_2^- production	NO_3^- production	PO_4^{3-} consumption
Temperature 20°C (long-term operation and start for short-term changes)	*15.9 (18.0)*	*1.1 (1.1)*	*10.0 (14.4)*	*142 (156)*
Temperature 15°C (one cycle change)	13.6 (11.7)	1.0 (1.2)	9.6 (8.8)	115 (134)
Temperature 15°C (long-term operation)	15.7 (16.8)	1.1 (2.1)	10.4 (13.6)	135 (151)
Temperature 8°C (one cycle change)	9.8 (8.2)	0.8 (0.8)	7.4 (6.5)	84 (94)
Temperature 8°C (long-term operation)	10.6 (13.6)	0.9 (0.7)	9.5 (11.9)	103 (109)

The short-term changes are simulated with the biomass distribution as developed at 20°C. Rates are calculated from the slopes of the simulated and experimentally determined concentration profiles in the reactor during a cycle. Experimental data are shown between parentheses (partly from De Kreuk et al., 2005b).

DOI 10.1002/bit

long-term simulations do not differ largely. This shows that the granules are adapting to a small temperature change if the time is long enough. The PAO population increases slightly at lower temperatures, leading to a faster phosphate consumption rate during the long-term experiment at 8°C than during the short-term experiment.

Similar to the results of simulations with different oxygen concentrations, enrichment of PAO and ammonia oxidizers can be explained by the higher oxygen penetration depth during the first period of the cycle. Increased oxygen penetration at lower temperatures is due to decreased activity of the organisms in the outer layers (Fig. 3i).

Influence of Granule Diameter on Nutrient Removal Efficiency

In the laboratory scale experiments, it was found that the average granule diameter fluctuated in time between 0.4 and 2 mm. This granule diameter is not controllable in current systems, but experimental data strongly suggests that it is correlated with nutrient removal (De Kreuk et al., 2005a and Fig. 4 here). In order to evaluate how sensitive this model is for granule size, spherical particles with diameters in the range from 0.72 to 1.61 mm were used in the simulations. In order to keep the total volume of the granules the same in all simulations (0.43 L), the number of granules (NG) was varied as well (NG between 197,000 and 2,190,000 particles). Reactor operation for every diameter was simulated for 365 days, each time starting with initial conditions.

The N-removal followed in general the trends as found in the experiments. However, the effect of granule diameter on N-removal in the simulations was smaller than measured in practice (Fig. 4a). Reading these figures, it should be noted that, due to the cycles in the SBR, a relatively small difference in conversion rate could result in much higher or lower effluent concentrations and thus in a significant difference in removal efficiency. For example, at the simulated diameter of 1.6 mm, an increased ammonia consumption rate from the present 12–14 mg $N \cdot L^{-1} \cdot h^{-1}$ would lead to an increased N-removal efficiency from 71% to 83%.

At small granule diameters, there is a large surface area to biomass volume ratio. Therefore, oxygen penetrates relatively deep into the granules. This leads to sufficient aerobic volume for a fast oxidation of ammonia. However, as soon as all ammonia and phosphate are removed from the system, oxygen will diffuse through the whole granule and denitrification will be inhibited. Therefore, at the same oxygen concentration overall N-removal efficiency will be lower at smaller diameters. When the diameter is larger than 1.4 mm, both N- and P-removal efficiencies start decreasing. At this granule size, the surface area becomes limiting for oxygen transport and thus for the conversion processes. This leads to a decreased ammonia oxidation rate and phosphate uptake rate and to ammonia and phosphate in the effluent. Simulations and experiments reveal that the optimum diameter for nutrient removal in the standard case operating conditions will be between 1.2 and 1.4 mm.

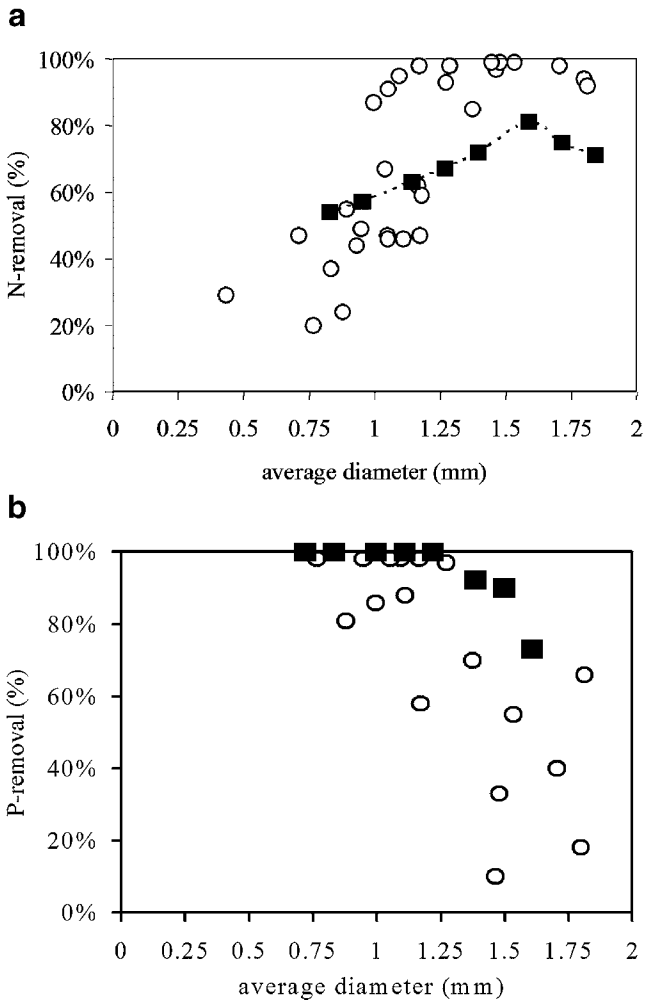

Figure 4. N-removal (**a**) and P-removal efficiency (**b**) at different average granule diameters: measured data (○, De Kreuk et al., 2005a) and data from several simulations (■).

Influence of Sludge Load on Nutrient Removal

In practice wastewater treatment plants are confronted with night and day fluctuations, dry weather and storm water influent, all leading to fluctuations in the sludge loading of the aerobic granules. Also industrial wastewaters are often more concentrated than sewage. The model was further used to study the optimum COD loading for nutrient removal. Sludge loading was varied by changing the amount of granules in the system (NG from 375,000 to 1,200,000), leading to a variation in sludge loading from 17.7 to 5.5 kg $COD \cdot m^{-3}_{granules} \cdot d^{-1}$ or loading rate of 0.8 to 2.5 kg $COD \cdot m^{-3}_{reactor} \cdot d^{-1}$. Every sludge-loading rate was applied for 365 days in simulations starting with the initial conditions described in the simulation strategy section.

From the simulations (Fig. 5), it can be observed that the N-removal efficiency slightly increases

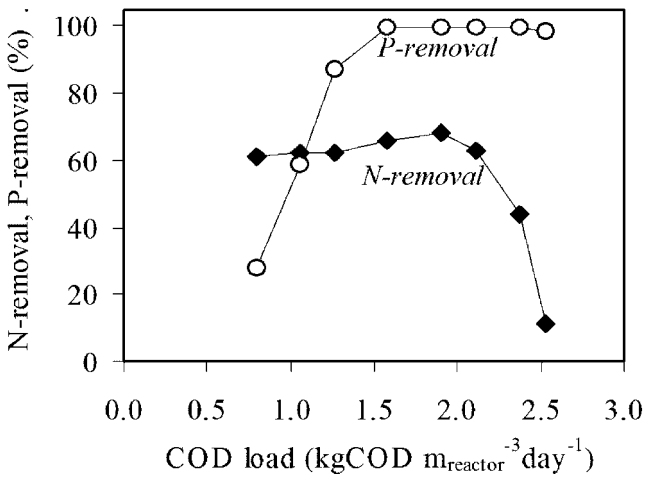

Figure 5. Influence of COD loading (in COD per m^3 reactor volume per day) on the N-removal efficiency (◆) and P-removal efficiency (○).

with an increasing load, with an optimum of 1.9 kgCOD $\cdot$ m^{-3} $\cdot$ d^{-1}, corresponding to a sludge loading rate of 13 kgCOD $\cdot$ m$_{granules}^{-3}$ $\cdot$ d^{-1}. At higher sludge loading rates, the N-removal efficiency quickly deteriorates. At very low sludge loading rates, ammonia is quickly oxidized to nitrate. As soon as all ammonia is converted, the oxygen uptake rate decreases, resulting in a fully aerobic granule and thus in limited denitrification during the rest of the cycle. The higher the sludge loading, the longer it takes to consume all ammonia and thus the anoxic zones in the granule exist during a longer part of the cycle. This results in more N-removal via denitrification at high sludge loading rates. However, at sludge loading rates higher than 1.9 kg $\cdot$ m^{-3} $\cdot$ d^{-1}, the amount of ammonium oxidizers is too low relative to the incoming ammonium, resulting in ammonium in the effluent. This leads to a fast decrease in the N-removal efficiency and accumulation of ammonium in the system.

Phosphate removal efficiency shows the opposite trend of the ammonium removal. At loading rates lower than 1.3kgCOD $\cdot$ m^{-3} $\cdot$ d^{-1} (corresponding to 9 kg $\cdot$ m$_{granules}^{-3}$ $\cdot$ d^{-1}), the phosphate removal efficiency decreases. This can be explained by the fact that a decreased COD loading rate reduces the concentration of PHB accumulated in the granules (in the anaerobic phase). In turn, less PHB causes slower biomass growth rates and in consequence an increasing sludge age. For example, the solid retention time (SRT) or sludge age at sludge loading rates 11 and 9 kg $\cdot$ m$_{granules}^{-3}$ $\cdot$ d^{-1} are, respectively, 20 and 38 days. Since phosphate can only be removed with the biomass in the effluent, a long SRT results in an insufficient phosphate removal from the system. As the poly-P concentrations in the biomass increase to high values, the rates of poly-P storage will become too low to remove all phosphate from the influent, resulting finally in accumulation of phosphate in the reactor and in the effluent.

Cycle Optimization; the Effect of an Extra Denitrification Period

Given the fact that ammonia and phosphate are both fully converted before the end of the SBR cycle and that nitrate accumulates in the standard operation (Fig. 2), an extra anoxic phase after the aeration period could increase the total N-removal efficiency. In order to study this effect of a denitrification period at the end of the cycle, one simulation was performed with a 90 min aeration period, followed by an anoxic period of 22 min, instead of the normal aeration period of 172 min. Especially the denitrification capacity with the remaining stored PHB was studied.

Since all phosphate is already consumed after the first hour of aeration, the anoxic period did not negatively influence the overall phosphate removal efficiency. It did, however, increase the N-removal efficiency to 80%, by significantly reducing nitrate concentration in the effluent (Fig. 6). This simulation showed that during the anoxic phase ammonia slightly increased due to biomass decay processes. Of the total incoming ammonium, 17% was discharged in the effluent as nitrate and 3% as ammonium. During the simulation of optimized SBR cycle, only very small changes were found in the pools of storage products, so the extra denitrification is not much affecting the PHB, glycogen, poly-P or the PAO concentrations in the granules. Therefore, it can be concluded that an extra denitrification period after the aerobic phase would be a logical step in the process optimization.

Discussion

In general, the mathematical model developed here described the experimental data well. However, an absolute prediction of the process with this model is difficult. Scenario analysis clearly showed that a small decrease in a

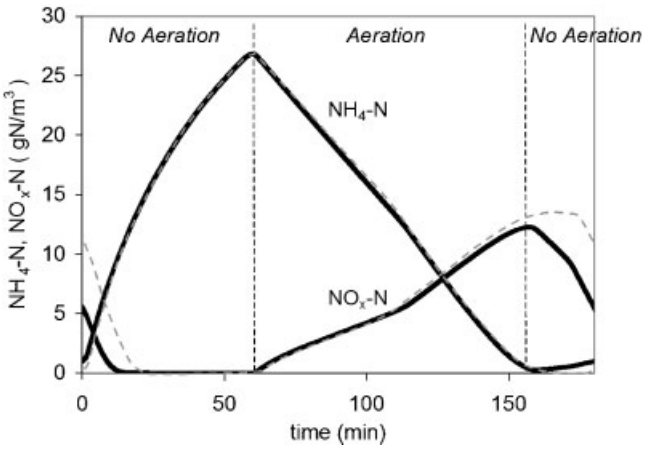

Figure 6. Simulated effect of an extra denitrification period at the end of the SBR cycle on the concentration profiles of N compounds (dotted lines: the standard cycle operation, solid lines: optimised cycle).

DOI 10.1002/bit

conversion rate can easily lead to an increased concentration of that component in the effluent. Because the model is based on a SBR system, this component will accumulate during the next cycles, leading to effluent data incomparable to experimental results. However, the trends of the conversion rates are comparable to practice, so the model can be used to obtain insight in the process rates and in the granule structure.

The main reason for the model to be less predictive is the complexity of the granular sludge itself. First of all, the granules in the model are of a certain diameter and are assumed to be perfect spheres. In reality, we are facing a wide range of granule sizes and shapes in a reactor (De Kreuk and Van Loosdrecht, 2004; Etterer and Wilderer, 2001; Toh et al., 2003). Less regularly shaped granules will lead to an increased surface to volume ratio, this influencing accordingly the oxygen transport into the granules. As can be seen from the simulations, mass transfer (especially the oxygen penetration in the granule) is decisive for the overall performance of the (simulated) system. It is possible to include several biofilm compartments with different granule diameters in AQUASIM, in order to simulate a granule size distribution, but this will make the model implementation and the interpretation of the data rather complex and will drastically increase the needed calculation time. Diffusive mass transport has never been a direct problem in ASMs, because in these models biomass is assumed in suspension in the bulk liquid. Consequently, nitrification and denitrification occur in different compartments, rather than simultaneously in the same reactor due to oxygen limitation in aerobic granules. This increases the ability of ASMs to predict effluent concentrations and overall system performance compared with the aerobic granular sludge systems.

When an aerobic granular sludge model must describe the behavior of this system in practice, like the ASM models, more system variables are needed due to the high complexity of the wastewater composition. In practice, the COD in the wastewater will partly consist of suspended COD. This needs to be hydrolyzed first, before organisms can use it for growth. Incorporating this substrate in the model implies the incorporation of heterotrophic biomass as well, since this relatively slow hydrolysis process will result in cell-external substrate during the aerobic period and thus to heterotrophic growth (McSwain et al., 2004; Schwarzenbeck et al., 2005). However, the exact rates and methods of conversion of suspended solids in aerobic granules are yet unknown, so more laboratory research will be needed first.

The granular sludge model was useful to obtain more insight in the biomass distribution within the granules. The increased concentration of autotrophic organisms in the outer layers of the granules and their shift to deeper layers when oxygen is available correspond to the hypothesis made from analyzing the experimental results. The trends in nutrient removal at varying granule diameter were also similar to the trends we found in practice. Simulation indicated that in the standard operating conditions (DO concentration 2 mg/L) the surface to volume ratio of aerobic granular sludge has its optimum at 600–700 m^2/m^3 reactor (corresponding to a granule diameter between 1.2 and 1.4 mm). Higher granule diameters lead to a permanent anaerobic core inside the granules and not enough autotrophic biomass in the outer aerobic layers resulting in ammonia in the effluent. The duration of an anaerobic core existence within an SBR cycle also plays a crucial role in the N-removal at different biomass loading rates. The longer the anaerobic zone exists, the longer denitrification takes place and the higher the N-removal efficiency. As in activated sludge systems with biological phosphate removal, the phosphate removal efficiency in aerobic granules is depending on the sludge age because poly-P leaves the system incorporated in the biomass. By extrapolation, we estimate that when the SRT exceeds 30 days the amount of phosphate removed from the reactor with the biomass is less than the incoming phosphate and phosphate will be found in the effluent.

Optimization of nutrient removal efficiencies involves the cycle optimization. As it becomes clear from the simulations, the oxygen penetration depth plays a major role. The oxygen concentration in the bulk liquid could be stepwise controlled via the oxygen uptake rate. If the oxygen uptake rate decreases, it means that oxygen penetration depth increases. Lowering the oxygen concentration in the bulk when the oxygen uptake rate decreases is expected to lead to a better overall N-removal efficiency. A more simple solution is the incorporation of denitrification steps in the cycle as shown by simulations. The model could be useful to determine at which moment in the cycle the anoxic period would be most effective. Simulations suggest that at the end of the cycle the PHB pool needed for denitrification is still sufficient, increasing the possibilities of timing this denitrification period.

Conclusions

The presented model describes the performance of a laboratory scale SBR, fed with defined influent, capable of simultaneously removing COD, nitrogen and phosphate in one reactor. The model describes the experimental data from this complex system sufficiently well, as the simulated trends in nutrient removal were similar to those obtained with laboratory experiments. Simulation results underline the importance of oxygen penetration depth into the granules, and thus the ratio of anoxic and aerobic biomass, for overall nutrient removal. The model can be used for process understanding and thus for optimization of the nutrient removal efficiency. It could also form a starting point for models to design full-scale treatment plants.

This research was funded by the Dutch Foundation for Wat. Res. (STOWA, TNW99.262) and STW (DPC5577) within the framework of the "aerobic granule reactors" project. The project is in close co-operation with DHV-Water in Leusden, The Netherlands. J. B. Xavier was financially supported by the FCT/MCTES, Portugal, through the Grant SFRH/BPD/11485/2002.

Biotechnology and Bioengineering, Vol. 97, No. 4, July 1, 2007

Appendix 1: Stoichiometry and Rates for the Bioconversion Processes Considered in the Model

		S_{O_2}	S_{Ac}	S_{NH_4}	S_{NO_3}	S_{NO_2}	S_{N_2}	S_{PO_4}	X_{PAO}	X_{PP}	X_{PHB}	X_{GLY}	X_{NH}	X_{NO}	X_I	
Process	Component	gO_2/m^3	$gCOD/m^3$	gN/m^3	gN/m^3	gN/m^3	gN/m^3	gP/m^3	$gCOD/m^3$	gP/m^3	$gCOD/m^3$	$gCOD/m^3$	$gCOD/m^3$	$gCOD/m^3$	$gCOD/m^3$	Rate
Phosphate accumulating organisms (PAO)																
	Anaerobic															
1	Storage of acetate		−1					Y_{PO_4}		Y_{PO_4}	$-Y_{PHB}$	$-(Y_{PHB}^{-}1)$				r_{SA}^{AN}
2	Maintenance							1		−1						r_{M}^{AN}
	Aerobic															
3	Consumption of PHB	$-(1-1/Y_{PHBO})$		$-i_{NBM}/Y_{PHBO}$				$-i_{PBM}/Y_{PHBO}$	$1/Y_{PHBO}$		−1					r_{PHB}^{O}
4	Storage of poly-P	$-1/Y_{PPO}$		i_{NBM}/Y_{PPO}				$-(1-i_{PBM}/Y_{PPO})$	$-1/Y_{PPO}$	1						r_{PP}^{O}
5	Glycogen formation	$1-1/Y_{GLYO}$		i_{NBM}/Y_{GLYO}				i_{PBM}/Y_{GLYO}	$-1/Y_{GLYO}$			1				r_{GLY}^{O}
6	Maintenance	−1		i_{NBM}				i_{PBM}	−1							r_{M}^{O}
	Anoxic (NO_3)															
7	Consumption of PHB			$-i_{NBM}/Y_{PHBNO_3}$	$-(1-1/Y_{PHBNO_3})/2.86$		$-(1-1/Y_{PHBNO_3})/2.86$	i_{PBM}/Y_{PHBNO_3}	$1/Y_{PHBNO_3}$		−1					$r_{PHB}^{NO_3}$
8	Storage of poly-P			i_{NBM}/Y_{PPNO_3}	$-1/(Y_{PPNO_3}\times 2.86)$		$1/(2.86\times Y_{PPNO_3})$	$-(1-i_{PBM}/Y_{PPNO_3})$	$-1/Y_{PPNO_3}$	1						$r_{PP}^{NO_3}$
9	Glycogen formation			i_{NBM}/Y_{GLYNO_3}	$(1-1/Y_{GLYNO_3})/2.86$		$-(1-1/Y_{GLYNO_3})/2.86$	i_{PBM}/Y_{GLYNO_3}	$1/Y_{GLYNO_3}$			1				$r_{GLY}^{NO_3}$
10	Maintenance			i_{NBM}	−1/2.86		1/2.86	i_{PBM}	−1							$r_{M}^{NO_3}$
	Anoxic (NO_2)															
11	Consumption of PHB			$-i_{NBM}/Y_{PHBNO_2}$		$-(1-1/Y_{PHBNO_2})/1.71$	$(1-1/Y_{PHBNO_2})/1.71$	$-i_{PBM}/Y_{PHBNO_2}$	$1/Y_{PHBNO_2}$		−1					$r_{PHB}^{NO_2}$
12	Storage of poly-P			i_{NBM}/Y_{PPNO_2}		$-1/(Y_{PPNO_2}\times 1.71)$	$1/(Y_{PPNO_2}\times 1.71)$	$-(1-i_{PBM}/Y_{PPNO_2})$	$-1/Y_{PPNO_2}$	1						$r_{PP}^{NO_2}$
13	Glycogen formation			i_{NBM}/Y_{GLYNO_2}		$(1-1/Y_{GLYNO_2})/1.71$	$-(1-1/Y_{GLYNO_2})/1.71$	i_{PBM}/Y_{GLYNO_2}	$1/Y_{GLYNO_2}$			1				$r_{GLY}^{NO_2}$
14	Maintenance			i_{NBM}		−1/1.71	1/1.71	i_{PBM}	−1							$r_{M}^{NO_2}$
	Decay															
15	Decay		$1-f_{XI}$	$i_{NBM}-i_{NXI}\times f_{XI}$				$i_{PBM}-i_{PXI}\times f_{XI}$	−1						f_{XI}	r_{D}
Autotrophic organisms																
	Nitrification (X_{NH})															
16	Growth	$-(3.43/Y_{NH}-1)$		$-1/Y_{NH}-i_{NBM}$		1/(Y_{NH})							1			$r_{G,NH}^{O}$
17	Aerobic end. resp.	$-(1-f_{XI})$		$i_{NBM}-i_{NXI}\times f_{XI}$									−1		f_{XI}	$r_{ER,NH}^{O}$
18	Anoxic end. resp.			$i_{NBM}-i_{NXI}\times f_{XI}$	$-(-f_{XI})/2.86$		$(1-f_{XI})/2.86$						−1		f_{XI}	$r_{ER,NH}^{NO_3}$
	Nitrification (X_{NO})															
19	Growth	$-(1.14/Y_{NO}-1)$			$1/Y_{NO}$	$-1/Y_{NO}-i_{NBM}$								1		$r_{G,NO}^{O}$
20	Aerobic end. resp.	$-(1-f_{XI})$		$i_{NBM}-i_{NXI}\times f_{XI}$										−1	f_{XI}	$r_{ER,NO}^{O}$
21	Anoxic end. resp.			$i_{NBM}-i_{NXI}\times f_{XI}$	$-(1\text{-}f_{XI})/2.86$		$(1-f_{XI})/2.86$							−1	f_{XI}	$r_{ER,NO}^{NO_3}$

(*Continued*)

DOI 10.1002/bit

Appendix 1: (*Continued*)

	Process		Process rate
Phosphate accumulating organisms			
	Anaerobic		
1	Storage of acetate	r_{SA}^{AN}	$q_{s,max} \cdot \frac{f_{PHB,max} - f_{PHB}}{(f_{PHB,max} - f_{PHB}) + K_{PHBP}} \cdot \frac{S_{Ac}}{S_{Ac} + K_{AcP}} \cdot X_{PAO}$
2	Maintenance	r_{M}^{AN}	$m_{An} \cdot \frac{K_{O_2,P}}{S_{O_2} + K_{O_2,P}} \cdot \frac{K_{NO_3,P}}{S_{NO_3,P} + K_{NO_3,P}} \cdot \frac{K_{NO_2,P}}{S_{NO_2} + K_{NO_2,P}} \cdot X_{PAO}$
	Aerobic		
3	Consumption of PHB	r_{PHB}^{O}	$z_{O_2} \cdot z_{NH_4} \cdot k_{PHB} \cdot \frac{f_{PHB}}{f_{PHB} + K_{fPHB,P}} \cdot \frac{S_{PO_4}}{S_{PO_4} + K_{PO_4}} \cdot \frac{S_{O_2}}{S_{O_2} + K_{O_2,P}} \cdot X_{PAO}$
4	Storage of poly-P	r_{PP}^{O}	$z_{O_2} \cdot \frac{X_{PAO}}{X_{PP}} \cdot k_{PP} \cdot \frac{f_{PP,max} - f_{PP}}{(f_{PP,max} - f_{PP}) + K_{PP,P}} \cdot \frac{S_{PO_4}}{S_{PO_4} + K_{PO_4,P}} \cdot \frac{S_{O_2}}{S_{O_2} + K_{O_2,P}} \cdot X_{PAO}$
5	Glycogen formation	r_{GLY}^{O}	$z_{O_2} \cdot \frac{X_{PHB}}{X_{GLY}} \cdot k_{GLY} \cdot \frac{f_{GLY,max} - f_{PP}}{(f_{GLY,max} - f_{GLY}) + K_{GLY,P}} \cdot \frac{S_{O_2}}{S_{O_2} + K_{O_2,P}} \cdot X_{PAO}$
6	Maintenance	r_{M}^{O}	$m_{O_2} \cdot \frac{S_{O_2}}{S_{O_2} + K_{O_2,P}} \cdot X_{PAO}$
	Anoxic (NO_3)		
7	Consumption of PHB	$r_{PHB}^{NO_2}$	$z_{NO_3} \cdot z_{NH_4} \cdot k_{PHB} \cdot \eta_{P,NO_3} \cdot \frac{f_{PHB}}{f_{PHB} + K_{fPHB,P}} \cdot \frac{S_{PO_4}}{S_{PO_4} + K_{PO_4}} \cdot \frac{S_{NO_3}}{S_{NO_3} + K_{NO_3,P}} \cdot \frac{K_{O_2,P}}{S_{O_2} + K_{O_2,P}} \cdot X_{PAO}$
8	Storage of poly-P	$r_{PP}^{NO_2}$	$z_{NO_3} \cdot \frac{X_{PAO}}{X_{PP}} \cdot k_{PP} \cdot \eta_{P,NO_3} \cdot \frac{f_{PP,max} - f_{PP}}{(f_{PP,max} - f_{PP}) + K_{PP,P}} \cdot \frac{S_{PO_4}}{S_{PO_4} + K_{PO_4,P}} \cdot \frac{S_{NO_3}}{S_{NO_3} + K_{NO_3,P}} \cdot \frac{K_{O_2,P}}{S_{O_2} + K_{O_2,P}} \cdot X_{PAO}$
9	Glycogen formation	$r_{GLY}^{NO_2}$	$z_{NO_3} \cdot \frac{X_{PHB}}{X_{GLY}} \cdot k_{GLY} \cdot \eta_{P,NO_3} \cdot \frac{f_{GLY,max} - f_{GLY}}{(f_{GLY,max} - f_{GLY}) + K_{GLY,P}} \cdot \frac{S_{NO_3}}{S_{NO_3} + K_{NO_3,P}} \cdot \frac{K_{O_2,P}}{S_{O_2} + K_{O_2,P}} \cdot X_{PAO}$
10	Maintenance	$r_{M}^{NO_2}$	$z_{NO_3} \cdot m_{NO_3} \cdot \frac{S_{NO_3}}{S_{NO_3} + K_{NO_3,P}} \cdot \frac{K_{O_2,P}}{S_{O_2} + K_{O_2,P}} \cdot X_{PAO}$
	Anoxic (NO_2)		
11	Consumption of PHB	$r_{PHB}^{NO_3}$	$z_{NO_2} \cdot z_{NH_4} \cdot k_{PHB} \cdot \eta_{P,NO_2} \cdot \frac{f_{PHB}}{f_{PHB} + K_{fPHB,P}} \cdot \frac{S_{PO_4}}{S_{PO_4} + K_{PO_4}} \cdot \frac{S_{NO_2}}{S_{NO_2} + K_{NO_2,P}} \cdot \frac{K_{O_2,P}}{S_{O_2} + K_{O_2,P}} \cdot X_{PAO}$
12	Storage of poly-P	$r_{PP}^{NO_3}$	$z_{NO_2} \cdot \frac{X_{PAO}}{X_{PP}} \cdot k_{PP} \cdot \eta_{P,NO_2} \cdot \frac{f_{PP,max} - f_{PP}}{(f_{PP,max} - f_{PP}) + K_{PP,P}} \cdot \frac{S_{PO_4}}{S_{PO_4} + K_{PO_4,P}} \cdot \frac{S_{NO_2}}{S_{NO_2} + K_{NO_2,P}} \cdot \frac{K_{O_2,P}}{S_{O_2} + K_{O_2,P}} \cdot X_{PAO}$
13	Glycogen formation	$r_{GLY}^{NO_3}$	$z_{NO_2} \cdot \frac{X_{PHB}}{X_{GLY}} \cdot k_{GLY} \cdot \eta_{P,NO_2} \cdot \frac{f_{GLY,max} - f_{GLY}}{(f_{GLY,max} - f_{GLY}) + K_{GLY,P}} \cdot \frac{S_{NO_2}}{S_{NO_2} + K_{NO_2,P}} \cdot \frac{K_{O_2,P}}{S_{O_2} + K_{O_2,P}} \cdot X_{PAO}$
14	Maintenance	$r_{M}^{NO_3}$	$z_{NO_2} \cdot m_{NO_2} \cdot \frac{S_{NO_2}}{S_{NO_2} + K_{NO_2,P}} \cdot \frac{K_{O_2,P}}{S_{O_2} + K_{O_2,P}} \cdot X_{PAO}$
	Decay		
15	Decay	r_{D}	$b_{PAO} \cdot \frac{K_{PHB,P}}{f_{PHB} + K_{fPHB,P}} \cdot \frac{K_{GLY,P}}{f_{GLY} + K_{GLY,P}} \cdot \frac{K_{Ac,P}}{S_{Ac} + K_{Ac,P}} \cdot X_{PAO}$
Autotrophic organisms			
	Nitrification (X_{NH})		
16	Growth	$r_{G,NH}^{O}$	$z_{O_2} \cdot z_{NH_4} \cdot \mu_{NH} \cdot \frac{S_{NH_4}}{S_{NH_4} + K_{NH_4,NH}} \cdot \frac{S_{O_2}}{S_{O_2} + K_{O_2,NH}} \cdot X_{NH}$
17	Aerobic end. resp.	$r_{ER,NH}^{O}$	$z_{O_2} \cdot b_{NH} \cdot \frac{S_{O_2}}{S_{O_2} + K_{O_2,NH}} \cdot X_{NH}$
18	Anoxic end. resp.	$r_{ER,NH}^{NO_3}$	$z_{NO_3} \cdot b_{NH} \cdot \eta_{NH,NO_3} \cdot \frac{S_{NO_3}}{S_{NO_3} + K_{NO_3,NH}} \cdot \frac{K_{O_2,NH}}{S_{O_2} + K_{O_2,NH}} \cdot X_{NH}$
	Nitrification (X_{NO})		
19	Growth	$r_{G,NO}^{O}$	$z_{O_2} \cdot z_{NO_2} \cdot \mu_{NO} \cdot \frac{S_{NO_2}}{S_{NO_2} + K_{NO_2,NO}} \cdot \frac{S_{O_2}}{S_{O_2} + K_{O_2,NO}} \cdot X_{NO}$
20	Aerobic end. resp.	$r_{ER,NO}^{O}$	$z_{O_2} \cdot b_{NO} \cdot \frac{S_{O_2}}{S_{O_2} + K_{O_2,NO}} \cdot X_{NO}$
21	Anoxic end. resp.	$r_{ER,NO}^{NO_3}$	$z_{NO_3} \cdot b_{NO} \cdot \eta_{NO,NO_3} \cdot \frac{S_{NO_3}}{S_{NO_3} + K_{NO_3,NO}} \cdot \frac{K_{O_2,NO}}{S_{O_2} + K_{O_2,NO}} \cdot X_{NH}$

Note: the functions $z_i = 1/(1 + e^{-200 \times S_i + 4}) + 10^{-12}$ switch the reaction off for negative substrate concentrations S_i.

Appendix 2: Stoichiometric Coefficients for the Bioconversion Processes Shown in Appendix 1

Symbol	Definition	Value	Unit	Reference
Composition factors (X_{PAO},X_{NH}, X_{NO})				
i_{NBM}	Nitrogen content of biomass	0.07	$gN \cdot gCOD_{BM}^{-1}$	(1)
i_{NXI}	Nitrogen content of inert particulate COD	0.02	$gN \cdot gCOD_{XI}^{-1}$	(1)
i_{PBM}	Phosphorus content of biomass	0.02	$gP \cdot gCOD_{BM}^{-1}$	(1)
i_{PXI}	Phosphorus content of inert particulate COD	0.01	$gP \cdot gCOD_{XI}^{-1}$	(1)
Phosphate accumulating organisms (X_{PAO})				
f_{XI}	Fraction of inert COD generated in decay	0.1	$gCOD_{XI} \cdot gCOD_{XPAO}^{-1}$	(1)
Y_{PO_4}	Anaerobic yield for phosphate release	0.5	$gP \cdot gCOD_{SAc}^{-1}$	(2)
Y_{PHB}	Anaerobic yield for PHB formation	1.5	$gCOD_{PHB} \cdot gCOD_{SAc}^{-1}$	(2)
Y_{PHBO}	Aerobic yield for PHB degradation	1.39	$gCOD_{PHB} \cdot gCOD_{XPAO}^{-1}$	(3)
Y_{PPO}	Aerobic yield for poly-P formation	4.42	$gP \cdot gCOD_{XPAO}^{-1}$	(3)
Y_{GLYO}	Aerobic yield for glycogen formation	1.11	$gCOD_{GLY} \cdot gCOD_{XPAO}^{-1}$	(3)
Y_{PHBNO_3}	Anoxic yield for PHB degradation on nitrate	1.7	$gCOD_{PHB} \cdot gCOD_{XPAO}^{-1}$	(3)
Y_{PPNO_3}	Anoxic yield for poly-P formation on nitrate	3.02	$gP \cdot gCOD_{XPAO}^{-1}$	(3)
Y_{GLYNO_3}	Anoxic yield for glycogen formation on nitrate	1.18	$gCOD_{GLY} \cdot gCOD_{XPAO}^{-1}$	(3)
Y_{PHBNO_2}	Anoxic yield for PHB degradation on nitrite	1.7	$gCOD_{PHB} \cdot gCOD_{XPAO}^{-1}$	(3)
Y_{PPNO_2}	Anoxic yield for poly-P formation on nitrite	3.02	$gP \cdot gCOD_{XPAO}^{-1}$	(3)
Y_{GLYNO_2}	Anoxic yield for glycogen formation on nitrite	1.18	$gCOD_{GLY} \cdot gCOD_{XPAO}^{-1}$	(3)
Autotrophic organisms: ammonium oxidizers (X_{NH}) and nitrite oxidizers (X_{NO})				
f_{XI}	Fraction of inert COD generated in endogenous respiration	0.1	$gCOD_{XI} \cdot gCOD_{XNH,NO}^{-1}$	(1)
Y_{NH}	Yield for growth of ammonium oxidizers	0.15	$gCOD_{XNH} \cdot gN^{-1}$	(4)
Y_{NO}	Yield for growth of nitrite oxidizers	0.041	$gCOD_{XNO} \cdot gN^{-1}$	(4)

(1) Henze et al. (1999); (2) Smolders et al. (1994); (3) Murnleitner et al. (1997) (4) Wiesmann (1994).

DOI 10.1002/bit

Appendix 3: Kinetic Parameters for the Bioconversions Shown in Appendix 1

Symbol	Definition	Value	Unit	Ref.
Phosphate accumulating organisms (X_{PAO})				
b_{PAO}	Rate constant for lysis and decay	$0.4 \cdot e^{\theta_{PAO}(T-20)}$	$1/d$	(1)
$f_{GLY,max}$	Maximum ratio of stored glycogen and biomass	0.5	—	(2)
$f_{PHB,max}$	Maximum ratio of stored PHB and biomass	0.8	—	—
$f_{PP,max}$	Maximum ratio of stored Poly-P and biomass	0.65	—	—
k_{GLY}	Glycogen formation rate	$0.93 \cdot e^{\theta_{PAO}(T-20)}$	$gCOD_{GLY}^{2} \cdot gCOD_{PHA}^{-1} \cdot gCOD_{XPAO}^{-1} \cdot d^{-1}$	(2)
k_{PHB}	PHB degradation rate	$5.51 \cdot e^{\theta_{PAO}(T-20)}$	$gCOD \cdot gCOD^{-1} \cdot d^{-1}$	(2)
k_{PP}	Poly-P formation rate	$0.45 \cdot e^{\theta_{PAO}(T-20)}$	$gP^{2} \cdot gCOD^{-1} \cdot d^{-1}$	(3)
$K_{Ac,P}$	Half-saturation coefficient for acetate	4	$gCOD \cdot m^{-3}$	(4)
$K_{GLY,P}$	Half-saturation coefficient for glycogen	0.01	$gCOD \cdot m^{-3}$	(2)
$K_{NO_2,P}$	Half-saturation coefficient for nitrite	1	$gN \cdot m^{-3}$	—
$K_{NO_3,P}$	Half-saturation coefficient for nitrate	1	$gN \cdot m^{-3}$	—
$K_{O_2,P}$	Half-saturation coefficient for oxygen	0.2	$gO_2 \cdot m^{-3}$	(1)
$K_{PHB,P}$	Half-saturation coefficient for PHB	0.01	$gCOD \cdot m^{-3}$	(1)
K_{PO_4}	Half-saturation coefficient for phosphate for growth	0.001	$gP \cdot m^{-3}$	—
$K_{PO_4,P}$	Half-saturation coefficient for phosphate for Poly-P formation	1	$gP \cdot m^{-3}$	(2)
$K_{PP,P}$	Half-saturation coefficient for Poly-P	0.01	$gP \cdot m^{-3}$	(4)
m_{An}	Anaerobic maintenance	$0.05 \cdot e^{\theta_{PAO}(T-20)}$	$gP \cdot gCOD^{-1} \cdot d^{-1}$	(3)
m_{NO_2}	Anoxic maintenance on nitrite	$0.11 \cdot e^{\theta_{PAO}(T-20)}$	$gCOD \cdot gCOD^{-1} \cdot d^{-1}$	(3)
m_{NO_3}	Anoxic maintenance on nitrate	$0.11 \cdot e^{\theta_{PAO}(T-20)}$	$gCOD \cdot gCOD^{-1} \cdot d^{-1}$	(3)
m_{O_2}	Aerobic maintenance on oxygen	$0.06 \cdot e^{\theta_{PAO}(T-20)}$	$gO_2 \cdot gCOD^{-1} \cdot d^{-1}$	(3)
$q_{s,max}$	Maximum acetate consumption rate	$8 \cdot e^{\theta_{PAO}(T-20)}$	$gCOD \cdot gCOD^{-1} \cdot d^{-1}$	(2)
z_{NH_4}	Switching function for ammonium	$1/(1+e^{-200 \cdot S\_NH_4+4}) + 10^{-12}$	—	—
z_{NO_2}	Switching function for nitrite	$1/(1+e^{-200 \cdot S\_NO_2+4}) + 10^{-12}$	—	—
z_{NO_3}	Switching function for nitrate	$1/(1+e^{-200 \cdot S\_NO_3+4}) + 10^{-12}$	—	—
z_{O_2}	Switching function for oxygen	$1/(1+e^{-200 \cdot S\_O_2+4}) + 10^{-12}$	—	—
η_{P,NO_2}	Reduction factor under anoxic conditions (NO_2^-)	0.3	—	—
η_{P,NO_3}	Reduction factor under anoxic conditions (NO_3^-)	0.3	—	—
θ_{PAO}	Temperature coefficient	0.063	—	(8)
Autotrophic organisms: ammonium oxidizers (X_{NH}) and nitrite oxidizers (X_{NO})				
b_{NH}	Lysis and decay rate coefficient (X_{NH})	$0.1 \cdot e^{\theta_{NH}(T-20)}$	d^{-1}	(6)
b_{NO}	Lysis and decay rate coefficient (X_{NO})	$0.06 \cdot e^{\theta_{NO}(T-20)}$	d^{-1}	(6)
$K_{NH_4,NH}$	Half-saturation coefficient for ammonium (X_{NH})	2.4	$gN \cdot m^{-3}$	(6)
$K_{NO_2,NO}$	Half-saturation coefficient for nitrite (X_{NO})	0.238	$gN \cdot m^{-3}$	(5)
$K_{NO_3,NH}$	Half-saturation coefficient for nitrate inhibition of decay (X_{NH})	1.0	$gN \cdot m^{-3}$	—
$K_{NO_3,NO}$	Half-saturation coefficient for nitrate inhibition of decay (X_{NO})	1.0	$gN \cdot m^{-3}$	—
$K_{O_2,NH}$	Half-saturation coefficient for oxygen (X_{NH})	0.3	$gO_2 \cdot m^{-3}$	(6)
$K_{O_2,NO}$	Half-saturation coefficient for oxygen (X_{NO})	0.1	$gO_2 \cdot m^{-3}$	(5)
η_{NH,NO_3}	Reduction factor under anoxic conditions (X_{NH})	0.3	—	—
η_{NO,NO_3}	Reduction factor under anoxic conditions (X_{NO})	0.5	—	—
$\mu_{NH,max}$	Maximum specific growth rate (X_{NH})	$0.4 \cdot e^{\theta_{NH}(T-20)}$	d^{-1}	Half the value (6)
$\mu_{NO,max}$	Maximum specific growth rate (X_{NO})	$1.1 \cdot e^{\theta_{NO}(T-20)}$	d^{-1}	(6)
θ_{NH}	Temperature coefficient (X_{NH})	0.094	—	(7)
θ_{XO}	Temperature coefficient (X_{NO})	0.061	—	(7)

(1) Henze et al. (1999); (2) Meijer (2004); (3) Murnleitner et al. (1997); (4) Henze et al. (1999); (5) Wijffels and Tramper (1995); (6) Wiesmann (1994); (7) Hao et al. (2002a); (8) Henze et al. (2000).

Appendix 4: Other Parameters Used in the Simulations, With Values According to the Experimental Conditions

Symbol	Definition	Value	Unit
D	Diffusion coefficient in the granule	0.0002/water fraction	$m^2 \cdot d^{-1}$
D_{Ac}	Diffusion coefficient of acetate in the granule in the feeding phase	5*D	$m^2 \cdot d^{-1}$
NG	Number of granules[a]	600,000	—
r_{max}	Maximum radius of the granules[a]	0.0055	m
$S_{Ac,in}$	Influent concentration acetate	396	$gCOD \cdot m^{-3}$
$S_{NH_4,in}$	Influent concentration ammonia	50	$gN \cdot m^{-3}$
$S_{PO_4,in}$	Influent concentration phosphate	20	$gP \cdot m^{-3}$
t_{cycle}	Total cycle time[a]	0.125	days
$V_{reactor}$	Total reactor volume	0.003	m^3
$V_{biofilm}$	Volume of the biofilm compartment[c]	0.0015	m^3
ρ_X	Density of the biomass	350,000	$gCOD \cdot m^{-3}$
ρ_{PHB}	Density of the storage polymers (PHB, glycogen and poly-P)[b]	$1 \cdot 10^8$	$gCOD \cdot m^{-3}$

[a]This was the situation in the basic simulation of 365 days. In other simulations these data can vary according to the description in the text.
[b]The density of the storage polymers was chosen extremely high, since the volume taken up by the polymers is already included in the volume of biomass (Beun et al., 2001).
[c]The biofilm compartment in AQUASIM contains bulk liquid, biofilm water and biofilm biomass fractions.

References

Beun JJ, Hendriks A, van Loosdrecht MCM, Morgenroth M, Wilderer PA, Heijnen JJ. 1999. Aerobic granulation in a sequencing batch reactor. Water Res 33(10):2283–2290.

Beun JJ, Van Loosdrecht MCM, Heijnen JJ. 2001. N-removal in a granular sludge sequencing batch airlift reactor. Biotechnol Bioeng 75(1): 82–92.

De Bruin LMM, De Kreuk MK, van der Roest HFR, Van Loosdrecht MCM, Uijterlinde C. 2004. Aerobic granular sludge technology, alternative for activated sludge technology? Water Sci Technol 49(11–12): 1–9.

De Bruin LMM, Van der Roest HF, de Kreuk MK, Van Loosdrecht MCM. 2005. Promising results Pilot research aerobic granular sludge technology at WWTP Ede. In: Bathe S, de Kreuk MK, McSwain BS, Schwarzenbeck N, editors. Aerobic Granular Sludge. London, UK: IWA Publishing. p 135–142.

De Kreuk MK, Van Loosdrecht MCM. 2004. Selection of slow growing organisms as a means for improving aerobic granular sludge stability. Water Sci Technol 49(11–12):9–19.

De Kreuk MK, Heijnen JJ, van Loosdrecht MCM. 2005a. Simultaneous COD, nitrogen and phosphate removal by aerobic granular sludge. Biotechnol Bioeng 90(6):761–769.

De Kreuk MK, Pronk M, Van Loosdrecht MCM. 2005b. Formation of aerobic granules and conversion processes in an aerobic granular sludge reactor at moderate and low temperatures. Water Res 39(18):4476–4484.

Dulekgurgen E, Yesiladali K, Ovez S, Tamerler C, Artan N, Orhon D. 2003. Conventional morphological and functional evaluation of the microbial populations in a sequencing batch reactor performing EBPR. J Environ Sci Health Part a-Toxic/Hazardous Substances & Environ Eng 38(8):1499–1515.

Etterer T, Wilderer PA. 2001. Generation and properties of aerobic granular sludge. Water Sci Technol 43(3):19–26.

Hao X, van Loosdrecht MCM, Meijer SCF, Heijnen JJ, Qian Y. 2001. Model-based evaluation of denitrifying P removal in a two-sludge system. J Environ Eng 127(2):112–118.

Hao X, Heijnen JJ, Van Loosdrecht MCM. 2002aModel-based evaluation of temperature and inflow variations on a partial nitrification ANAMMOX biofilm process. Water Research 36(19):4839–4849.

Hao XD, Heijnen JJ, van Loosdrecht MCM. 2002b. Sensitivity analysis of a biofilm model describing a one-stage completely autotrophic nitrogen removal (CANON) process. Biotechnol Bioeng 77(3):266–277.

Henze M, Gujer W, Mino T, Matsuo T, Wentzel MC, Marais GvR, Van Loosdrecht MCM. 1999. Activated Sludge Model No.2d, ASM2D. Water Sci Technol 39(1):165–182.

Henze M, Gujer W, Mino T, van Loosdrecht M. 2000. Activated sludge models; ASM1, ASM2, ASM2d and A SM3. London: IWA Publishing. 130 p.

Li XM, Yang GJ, Yang Q, Zeng GM, Liao DX, Hu MF, Wu YM. 2005. Simultaneous phosphorus and nitrogen removal by aerobic granular sludge in single SBR system. In: Bathe S, De Kreuk MK, Mc Swain BS, Schwarzenbeck N, editors. Aerobic granular sludge. London, UK: IWA. p 71–78.

Liu Y, Tay J-H. 2004. State of the art of biogranulation technology for wastewater treatment. Biotechnol Adv 22(7):533–563.

Lübken M, Schwarzenbeck N, Wichern M, Wilderer PA. 2005. Modelling nutrient removal of an aerobic granular sludge lab-scale SBR using A SM3. In: Bathe S, De Kreuk MK, Mc Swain BS, Schwarzenbeck N, editors. Aerobic granular sludge. London, UK: IWA. p 103–110.

McSwain BS, Irvine RL, Wilderer PA. 2004. The effect of intermittent feeding on aerobic granule structure. Water Sci Technol 49(11):19–25.

Meijer SCF. 2004. Theoretical and practical aspects of modelling activated sludge processes [PhD.]. Delft: Technical University. 204 p

Morgenroth E, Sherden T, van Loosdrecht MCM, Heijnen JJ, Wilderer PA. 1997. Aerobic granular sludge in a sequencing batch reactor. Water Res 31(12):3191–3194.

Murnleitner E, Kuba T, van Loosdrecht MCM, Heijnen JJ. 1997. An integrated metabolic model for the aerobic and denitrifying biological phosphorus removal. Biotechnol Bioeng 54(5):434–450.

Reichert P. 1998. AQUASIM 2.0—Computer program for the Identification and Simulation of Aquatic Systems. Version 2.0. Dubendorf: EAWAG.

Schwarzenbeck N, Borges JM, Wilderer PA. 2005. Treatment of dairy effluents in an aerobic granular sludge sequencing batch reactor. Appl Microbiol Biotechnol 66(6):711–718.

Smolders GJF, van der Meij J, Van Loosdrecht MCM, Heijnen JJ. 1994. Model of the anaerobic metabolism of the biological phosphorus removal process; stoichiometry and pH influence. Biotechnol Bioeng 43:461–470.

Tay JH, Liu QS, Liu Y. 2002. Aerobic granulation in sequential sludge blanket reactor. Water Sci Technol 46(4–5):13–18.

Toh SK, Tay JH, Moy BYP, Ivanov V, Tay STL. 2003. Size-effect on the physical characteristics of the aerobic granule in a SBR. Appl Microbiol Biotechnol 60(6):687–695.

van Veldhuizen HM, van Loosdrecht MCM, Heijnen JJ. 1999. Modelling biological phosphorus and nitrogen removal in a full scale activated sludge process. Water Res 33(16):3459–3468.

DOI 10.1002/bit

Wanner O, Gujer W. 1986. A multispecies biofilm model. Biotechnol Bioeng 28(3):314–328.
Wentzel MC, Ekama GA, Loewenthal RE, Dold PL, Marais GR. 1989. Enhanced polyphosphate organism cultures in activated sludge systems. Part II: Experimental behavior. Water SA 15(2):71–88.
Wiesmann U. 1994. Biological nitrogen removal from wastewater. Adv Biochem Eng/Biotechnol 51:113–154.
Wijffels RH, Tramper J. 1995. Nitrification by immobilized cells. Enzyme and Microbial Technology 17(6):482–492.
Xavier JB, de Kreuk MK, Picioreanu C, Van Loosdrecht MCM. Submitted. Microbial populations dynamics and nutrient conversions in aerobic granular sludge described by multi-scale modelling. Environ Sci Technol.